Chemical Engineering Journal 159 (2010) 47–52

Contents lists available at ScienceDirect

Chemical Engineering Journal

journal homepage: www.elsevier.com/locate/cej

# Methyl orange degradation by pulsed discharge in the presence of activated carbon fibers

Yanzong Zhang, Baiye Sun, Shihuai Deng*, Yingjun Wang, Hong Peng, Yuanwei Li, Xiaohong Zhang

*Provincial Key Laboratory of Agricultural Environmental Engineering, College of Resources & Environment, Sichuan Agricultural University, Ya'an 625014, Sichuan, China*

ARTICLE INFO

*Article history:*
Received 2 November 2009
Received in revised form 5 February 2010
Accepted 8 February 2010

*Keywords:*
Surface modification
Adsorption
Catalysis
Synergistic effect

ABSTRACT

The effects of activated carbon fibers (ACF0, ACFH, and ACFN) on the degradation of methyl orange were investigated in a pulsed discharge reactor. ACF0 fibers were modified with nitric acid (to yield ACFH fibers) or ammonia (to yield ACFN fibers) to create fibers with different porous structures and chemical properties. The adsorption properties of ACF0, ACFH, and ACFN depended on their pore diameter, but the catalytic properties were independent of their chemical properties. Acidic and basic surfaces both accelerated ozone decomposition, resulting in formation of hydroxyl radicals. Boehm titration and Fourier-transform infrared spectral studies indicated that the numbers of acidic and basic groups on ACF0, ACFH, and ACFN surfaces could be increased by this process, as could the surface areas and pores volumes. ACF0, ACFH, and ACFN could also be regenerated *in situ* after repeated use.



## 1. Introduction

In recent years, there has been growing interest in the development of pulsed discharge methods for the degradation of colored wastewaters, including those containing reactive dyes and azo dyes [1–3]. The pulsed discharge process can generate a number of reactive chemical species in water, such as oxygen-containing radicals ($O^{\bullet}$, $HO^{\bullet}$) and active molecular species (e.g. $H_2O_2$, $H_2$, $O_3$) [4]. The process works primarily by oxidation and decomposition of organic pollutants in the water by these reactive chemical species, thus avoiding generation of secondary pollutants.

Recent studies [5–8] have reported that activated carbon (AC) can accelerate the production of $HO^{\bullet}$ radicals from ozone decomposition. Liquid-phase discharge reactors can also be configured to produce ozone by injection of oxygen (or air) across high-voltage hollow electrodes immersed in water [4], so there may be an advantage in using AC in combination with this process. Previous work [9,10] has shown that the combination of pulsed discharge and AC enhances overall removal of phenol from solution. A recent study [11] has indicated that this combined treatment has a synergistic effect on the degradation of dyes in wastewaters. The superiority of activated carbon fibers (ACF) over conventional AC can be seen from the micropore percentage and the narrow pore-size distribution. There may therefore be greater advantages to be obtained by adding ACF, rather than AC, to a pulsed discharge reactor system for decolorization processes. However, the combination of pulsed discharge and ACF has not yet been investigated in wastewater treatment.

The aim of the present research was therefore to evaluate the effects of ACF in a pulsed discharge decolorizing system, focusing on changes in the surface and chemical properties of the ACF. Methyl orange (MO), which has a relatively high toxicity, a complex structure, and high resistance to biodegradation, was chosen as the model contaminant because it can be classified as both an acid and an azo dyestuff, both of which are widely used in the textile industry.

## 2. Materials and methods

### 2.1. Materials

Commercial viscose-based ACF felt, supplied by the Zichuan Carbon Fiber Limited Company, Qinhuangdao, China, was cut into 3 mm × 3 mm pieces, rinsed with distilled water, and dried at 383 K for 24 h. This material was designated ACF0. An ACF0 sample was divided into two equal portions, and each portion was placed in a 200-mL jar, to which 10 M nitric acid or 10 M ammonia was added at a ratio of 10 mL $g^{-1}$ of felt. The jars were heated at 333 K for 6 h in a water bath equipped with a thermostat. The felt samples were then washed with distilled water until the pH was neutral, and dried in an oven at 383 K for 24 h. The felts modified by nitric acid and ammonia were designated ACFH and ACFN, respectively.

### 2.2. Analytical methods

Nitrogen adsorption isotherms were determined at 77 K using a Micrometrics ASAP 2000 analyzer (Micrometrics, Nor-

* Corresponding author. Tel.: +86 835 288 2210; fax: +86 835 288 2182.
*E-mail address:* zh.plasma@yahoo.com.cn (S. Deng).

1385-8947/$ – see front matter © 2010 Elsevier B.V. All rights reserved.
doi:10.1016/j.cej.2010.02.023

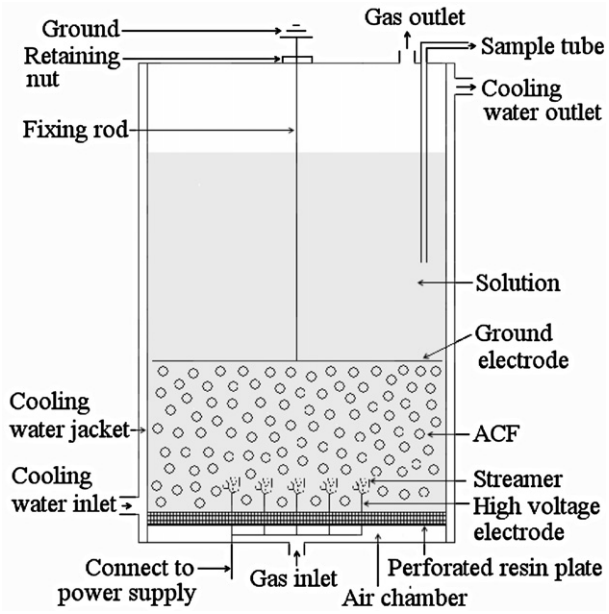


**Fig. 1.** Schematic of pulsed discharge reactor.

cross, GA, USA). The surface area was calculated using the Brunauer–Emmett–Teller (BET) model. The pore-volume and pore-size distributions were obtained using density function theory. Analysis of the ACF surface functionalities was carried out using Boehm's method [12]. The point of zero charge ($pH_{PZC}$) was measured by the mass titration/pH equilibration method [13]. Fourier-transform infrared spectra (FTIR) were recorded on a Nicolet Impact 380 spectrometer (ThermoNicolet, Madison, WI, USA) using KBr pellets.

The MO concentration was determined against a prepared standard curve by measuring the absorbance at 465 nm with an ultraviolet spectrophotometer (UV-762, Leici Limited Company, Shanghai, China). The MO solution pH and conductivity were measured using a PHSJ-3F pH meter and a DDB-11A conductivity meter (Leici Limited Company, Shanghai, China), respectively. The dissolved ozone concentration was determined by the standard iodometric method [14]. The synergy intensities and the regeneration percentages of ACF0, ACFH, and ACFN, and the energy efficiencies were calculated as described in previous work [11,15]. The chemical oxygen demand (COD) was measured with a CM-02 COD analyzer (Beijing Shuanghui Corp., China) using the acidic oxidation by dichromate method.

### 2.3. Experimental apparatus

The experimental apparatus consisted of a pulsed power supply which has been previously described [15], and a pulsed discharge reactor consisting of a 400 mL glass vessel with a cooling water jacket for temperature control. A high-voltage electrode was introduced into the reactor through a perforated resin plate at the bottom. A ground electrode was placed 9 mm above the high-voltage electrode. Oxygen was bubbled into the air chamber using a gas flowmeter, and then passed through the perforated resin plate into the discharge region. The sampling tube consisted of an injector and part of a transfusion system, which included a flexible pipe and a liquid filter. The reactor is shown in Fig. 1.

The reactor reference conditions were as follows: five acupuncture needles in parallel, with a needle spacing of 10 mm; an electrode gap of 9 mm; an input voltage of 46 kV, with 100 pulses $s^{-1}$; and an oxygen flow rate of 60 L $h^{-1}$. The reactor was filled with 200 mL MO solution (80 mg $L^{-1}$, pH 6.1, conductivity 20 μS $cm^{-1}$), either with or without 0.25 g ACF, and the power was applied. Samples from the reaction solution (5 mL) were taken for analysis at given intervals.

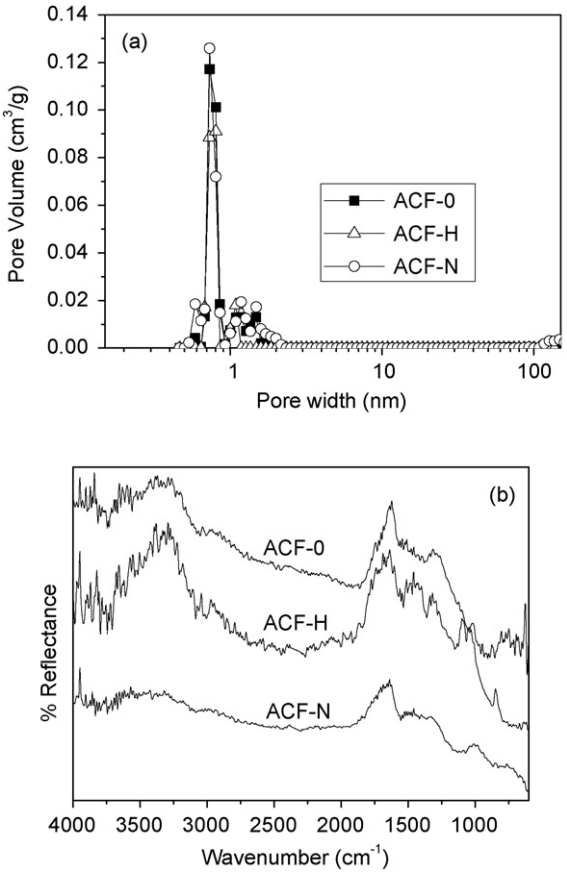


**Fig. 2.** (a) Pore-size distribution and (b) FTIR spectra of ACF0, ACFH, and ACFN.

The power supply applied a voltage to the high-voltage electrode and the ground electrode. Electric discharge occurred in the aqueous phase and in the gas phase when oxygen was bubbled into the discharge reactor. HO• radicals and $H_2O_2$ were produced in the liquid phase and ozone was generated in the gas phase. These active species reacted with organic pollutants and mineralized them to $H_2O$ and $CO_2$. ACF was added to the discharge reactor and suspended under vigorous stirring in a rising air flow. Synergistic combination between the pulsed discharge and the ACF occurred. The operating conditions were estimated by preliminary tests and the absence of diffusion limitations was verified.

## 3. Results and discussion

### 3.1. ACF pore structure and surface chemical characteristics

The pore structures and surface chemical characteristics of ACF0, ACFH, and ACFN are illustrated in Fig. 2. The isotherms are type I in the IUPAC classification system, indicating the dominant presence of micropores. The differences in ACF0, ACFH, and ACFN pore structures can be further deduced from Fig. 2a. The ACF0 pore-size distribution was 0.59–1.7 nm, with a peak at 0.7 nm. The ACFN pore-size distribution was 0.54–2.0 nm, with a peak at 0.7 nm. The ACFH pore-size distribution was 0.68–1.1 nm, with a peak at 0.8 nm.

The differences in the surface chemical characteristics of ACF0, ACFH, and ACFN can be deduced from the FTIR measurements shown in Fig. 2b. In the range 3600–3100 $cm^{-1}$, surface hydroxyl groups and chemisorbed water give rise to a band of O–H stretch-

**Table 1**
Pore structure and surface chemical characteristics of ACF samples.

| | Specific surface area ($m^2\,g^{-1}$) | Micropores volume ($cm^3\,g^{-1}$) | Mesopores volume ($cm^3\,g^{-1}$) | $pH_{PZC}$ | Acidic groups ($\mu mol\,g^{-1}$) | Basic groups ($\mu mol\,g^{-1}$) |
|---|---|---|---|---|---|---|
| ACF0 | 829 | 0.3093 | 0.0030 | 6.74 | 0.123 | 0.06 |
| ACFH | 629 | 0.2321 | 0.0024 | 6.22 | 0.247 | 0.00 |
| ACFN | 898 | 0.3271 | 0.0251 | 7.96 | 0.105 | 0.28 |
| Used ACF0 | 871 | 0.3259 | 0.0069 | 6.18 | 0.286 | 0.08 |
| Used ACFH | 762 | 0.2778 | 0.0072 | 5.84 | 0.446 | 0.03 |
| Used ACFN | 858 | 0.3241 | 0.0240 | 7.45 | 0.264 | 0.29 |

ing vibrations [16–17]. The peaks at 3024 and 2966 $cm^{-1}$ may be attributed to symmetrical and asymmetrical vibrations of aliphatic –CH, $–CH_2$ and $–CH_3$ groups [12,18]. The band at 1860–1650 $cm^{-1}$ corresponds to the stretching vibrations of C=O in carbonyl and carboxyl groups [19]. The peak centered at 1639 $cm^{-1}$ may result from the superposition of aromatic C=C stretching vibrations and C=O stretching vibrations in carboxyl, ester, lactone, and carbonyl groups [12,16]. The complex band between 1600 $cm^{-1}$ and 1400 $cm^{-1}$ can be attributed to stretching vibrations of aromatic C=C with various substituents [19]. The peaks between 1400 and 1300 $cm^{-1}$ may correspond to deformation vibrations of aromatic rings and O–H bending vibrations of carboxyl and hydroxyl groups [13,20]. The broad band at 1300–950 $cm^{-1}$ is compatible with C–O single-bond stretching vibrations in $\gamma$- and $\delta$-lactones, aromatic and aliphatic ethers, phenols, and epoxides [16,21]. The absorbance strips between 910 and 650 $cm^{-1}$ relate to inner and outer plane deformations of substituted benzene rings [22].

For ACFH, the broad band of O–H stretching vibrations in the range 3600–3100 $cm^{-1}$ is noticeably more extensive. The C=O vibrations of anhydride groups result in a broad band at 1740–1810 $cm^{-1}$, whereas the peaks due to "isolated" carboxyl and lactone groups should be sharper and more intense [23]. The carboxyl C=O stretching of an aromatic carboxylic acid generally appears at 1690 $cm^{-1}$ [19]. The peak at 1460 $cm^{-1}$ can be attributed to C=O and O–H bending vibration [19–20]. The peak at 1320 $cm^{-1}$ can be attributed to C–O deformation vibrations [20]. The band at 1045 $cm^{-1}$ and the shoulder at 1110 $cm^{-1}$ are attributable to C–O stretching vibrations [24]. The three bands at 880, 810, and 750 $cm^{-1}$ are assigned to ring substitutions. These band positions are characteristic of one to three adjacent hydrogen systems [12]. The peak at 605 $cm^{-1}$ can be attributed to out-of-plane bending vibrations of O–H.

In ACFN, there are obviously fewer acidic groups. The band due to nitrogen-containing species appears in the region 1750–1700 $cm^{-1}$ [17]. A band due to vibrations of pyridine-like structures or cyclic amides (–C=N–) appears in the region 1610–1480 $cm^{-1}$. The band in the region 1470–1380 $cm^{-1}$ may include C–N– vibrations in heterocyclic structures. The band in the region 1300–1000 $cm^{-1}$ may result from tertiary nitrogen species incorporated into the carbon structure. Cyclic compounds containing conjugated C=C and C=N may be responsible for the absorptions observed below 900 $cm^{-1}$.

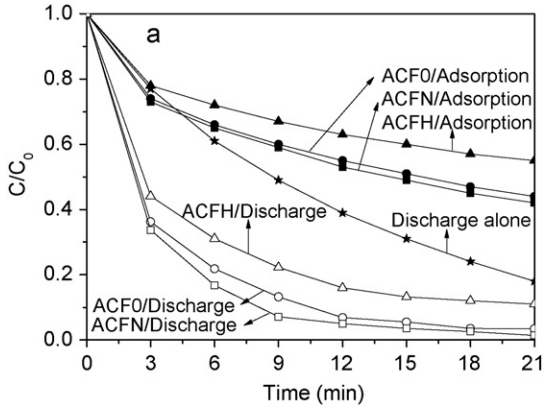


**Fig. 3.** Effect of ACF0, ACFH, and ACFN on MO removal in the absence and in the presence of pulsed discharge (initial solution pH 6.1 and conductivity 20 $\mu S\,cm^{-1}$).

Table 1 summarizes the various parameters of ACF0, ACFH, and ACFN. Nitric acid oxidation (ACFH) brought about a reduction in specific surface area, a reduction in micropore and mesopore volumes, and a large increase in the number of acidic groups, which resulted in a decrease in $pH_{PZC}$. The reduction in micropore and mesopore volumes may be due to acidic groups blocking partial micropores and mesopores [25]. After ammonia treatment (ACFN), specific surface area, micropore and mesopore volumes, and the number of basic groups increased, and the number of acidic groups decreased, which led to an increase in $pH_{PZC}$. This is a result of decomposition of partial acidic groups and formation of new basic nitrogen-containing functionalities [26].

### 3.2. Effects of ACF in the combined treatment

#### 3.2.1. Synergistic effects in the combined treatment

To determine the effect of ACF0, ACFH, and ACFN in the combined treatment, a set of control experiments was carried out with addition of ACF0, ACFH, or ACFN to the MO solution in the absence and in the presence of pulsed discharges, as shown in Fig. 3. The adsorption of MO on ACF0, ACFH, and ACFN in the absence of a pulsed discharge was found to depend on the pore diameter. The MO molecular size (calculated using Chemoffice software, CambridgeSoft, Cambridge, MA, USA) is 1.54 nm × 0.48 nm × 0.28 nm. For ACF0 and ACFN, MO molecules can be adsorbed with flat configurations (1.54 nm × 0.48 nm), oblique configurations (1.54 nm × 0.28 nm), and terminal group interactions (0.48 nm × 0.28 nm). For ACFH, MO molecules can only be adsorbed with flat and oblique configurations. The best adsorption was observed for ACFN because it had the greatest number of micropores, and the lowest adsorption was seen for ACFH because it had the fewest micropores. Fig. 3 also shows the existence of a synergistic effect in the combined treatment for ACF0, ACFH, and ACFN. As shown in Table 2, the synergy intensities were positive within 9 min for ACFN, and positive within 6 min for ACF0 and ACFH. This result indicates that the disappearance of MO molecules may result from catalysis by ACF0, ACFH, and ACFN as well as from adsorption.

In the present study, a discharge reactor energy efficiency of 6.36 $g\,kW^{-1}\,h^{-1}$ for the ACF/pulsed discharge combination was achieved. In a previous study, an energy efficiency of

**Table 2**
Synergy intensity of ACF samples in the combined treatment.

| | Time (min) | | | | | | |
|---|---|---|---|---|---|---|---|
| | 3 | 6 | 9 | 12 | 15 | 18 | 21 |
| ACF0 | 23.2 | 6.6 | −4.8 | −13.9 | −24.9 | −34.2 | −42.6 |
| ACFH | 19.5 | 2.8 | −8.1 | −16.7 | −25.6 | −35.2 | −42.7 |
| ACFN | 24.6 | 11.1 | 1 | −13.7 | −24.4 | −33.6 | −42.2 |

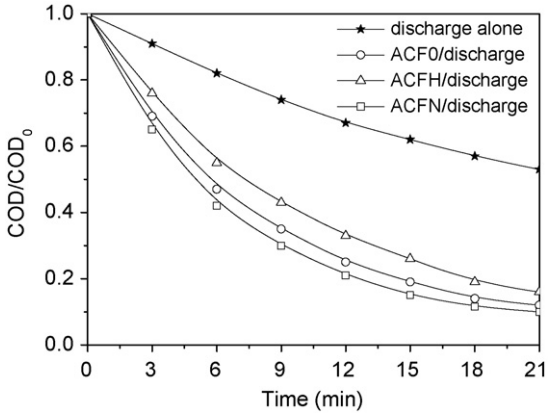


**Fig. 4.** COD removal in the presence of pulsed discharge (initial solution pH 6.1 and conductivity 20 μS cm$^{-1}$).

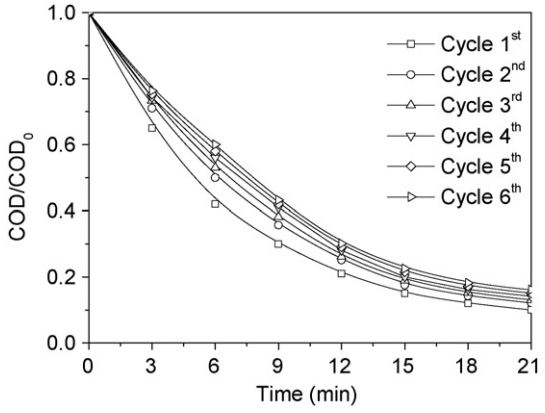


**Fig. 5.** Repeated use of ACFN for MO removal in the presence of pulsed discharge (initial solution pH 6.1 and conductivity 20 μS cm$^{-1}$).

4.66 g kW$^{-1}$ h$^{-1}$ was obtained for a pulsed discharge/AC combination [11]. Compared with the previous study (where the amount of AC was 1.2 g and the solution concentration was 60 mg L$^{-1}$), the solution concentration increased and the amount of AC decreased, but the energy efficiency of the discharge reactor increased by 34.5%. Thus the combination of pulsed discharge and ACF can be an effective approach to improving the overall energy efficiency of the discharge reactor.

### 3.2.2. COD removal in the combined treatment

COD removal was also examined to determine MO mineralization, as shown in Fig. 4. Fig. 4 illustrates that COD removal reached 47% using pulsed discharge alone. The reactor is designed so that it can use the ozone produced in pulsed discharge. Nevertheless, ozonation leads to the formation of by-products such as low molecular weight acids [27]. The by-products appear to be resistant to ozone attack. This indicates that ozonation is more efficient for decolorization than COD removal is. However, for the combination of pulsed discharge and ACF0, ACFH, or ACFN, COD removal increased to 88%, 84%, and 90%, respectively. It is obvious that the combined treatment significantly increased COD removal, and that low molecular weight acids were further mineralized to $H_2O$ and $CO_2$, which led to an increase in the pH and a decrease in the conductivity of the solution. The final pH values of the solutions were 4.38, 5.56, 5.40, and 5.60, and the final solution conductivities were 55, 27, 30, and 25 μS cm$^{-1}$, for discharge alone and in the presence of ACF0, ACFH, and ACFN, respectively.

### 3.2.3. Repeated use of ACF samples

To evaluate the type of contribution made by ACF0, ACFH, and ACFN to the combined treatment process, six cycles were performed with the same samples. This is shown in Fig. 5, using ACFN as an example. The trends for ACF0 and ACFH were similar to that for ACFN. COD removal was slightly lower in the second cycle than that in the first cycle. This difference may be because a fraction of the MO molecules adsorbed in the micropores of ACFN were not desorbed from the adsorption sites. COD removal was almost unchanged after the third cycle. This implies that adsorption of MO on ACFN in the combined treatment differs from that in the absence of a pulsed discharge. When the treatment time was extended, the synergy intensities in Table 2 decreased and quickly became negative. This is because most MO molecules have by then decomposed, which means that the probability of reacting with HO• radicals is reduced. However, HO• radicals react with by-products during this period and further mineralize them to $H_2O$ and $CO_2$.

Adsorption of ACFN on MO was also tested in the absence of a pulsed discharge under the same conditions. The results are shown in Fig. 6. COD removal was higher in the first and second cycles by adsorption of ACFN. As the number of cycles increased, the adsorption performance of ACFN decreased and almost reached saturation adsorption in the sixth cycle. By comparing COD removal with and without pulsed discharge (Figs. 5 and 6), it can be further affirmed that COD removal resulted from catalysis as well as from adsorption on ACFN.

### 3.2.4. ACF catalysis in the combined treatment

Recent studies [5–7] have reported that AC can accelerate ozone decomposition, resulting in the formation of HO• radicals. Basic AC performs better in this process. To investigate the effect of functional groups on the ACF surface in the combined treatment, the dissolved ozone concentration was measured after the reaction. The dissolved ozone concentration was 0.015 mM for discharge alone, but was 0.005, 0.006, and 0.005 mM in the presence of ACF0, ACFH, and ACFN, respectively. Thus, not only basic groups but also some types of acidic groups can react with ozone. A possible mechanism is that basic groups and some acidic groups on the ACF surface react with ozone by both electrophilic attack and cycloaddition, leading to dicarboxylic acids and $H_2O_2$ as by-products. $H_2O_2$ is then transformed to surface HO• radicals, catalyzed by the π-electrons of the basal planes [8]. Consequently, the combined treatment significantly increased COD removal. The increase in COD removal may be due to: (i) mineralization of both dyes and by-products to $H_2O$ and $CO_2$ by reactive species produced in the pulsed discharge and catalyzed by ACF; (ii) adsorption of a fraction of the dyes and by-products on ACF. ACF therefore acts

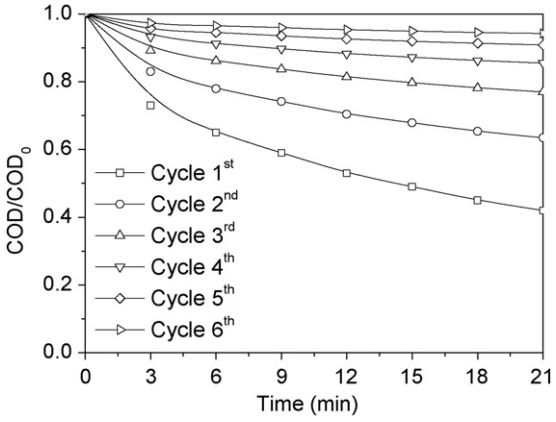


**Fig. 6.** Adsorption behavior of MO on ACFN in the absence of pulsed discharge (initial solution pH 6.1 and conductivity 20 μS cm$^{-1}$).

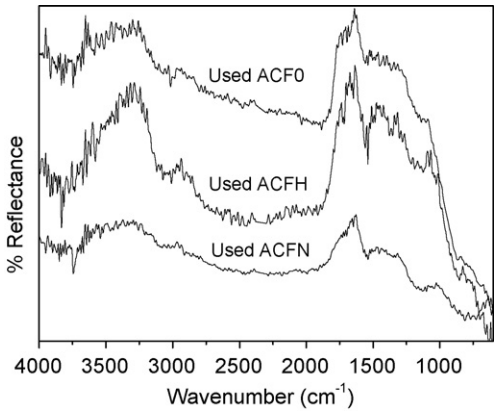


**Fig. 7.** FTIR spectra of ACF0, ACFH, and CFN after use.

not only as an adsorbent, but also as a catalyst during pulsed discharge.

### 3.3. Influence of pulsed discharge on pore structure and surface chemistry

The pore structures of ACF0, ACFH, and ACFN after use are shown in Table 1. The nitrogen adsorption isotherm type was unchanged. The micropore and mesopore volumes of ACF0 increased after use. This may reflect a reaction of the amorphous carbon on the ACF0 surface with oxygen atoms produced in the pulsed discharge, which leads to development of a microporous structure. In the latter phase of the reaction, the enlarging of existing pores and the formation of large pores by burnout of the walls between adjacent pores also takes place. The micropore and mesopore volumes of ACFH increased significantly after use. In addition to the reasons mentioned above, partial decomposition of the acidic groups directed away from the micropores may occur, which would enlarge these pores. The micropore and mesopore volumes of ACFN decreased slightly after use, which is attributed to the fixation of acidic groups produced inside these pores, which would effectively reduce their size.

The surface chemical characteristics of ACF0, ACFH, and ACFN after use are illustrated in Fig. 7 and Table 1. Comparison with Fig. 2b shows no new peaks in the range above 1000 $cm^{-1}$ in the used samples, only enhancement of the existing peaks, which indicated an increase in the number of acidic groups. This is in good agreement with the Boehm titration results. In the range below 1000 $cm^{-1}$, a new band appeared for ACFN, and a primary band disappeared for ACFH, which indicated that the benzene ring substituents derived from surface modification are unstable. The changes in the pore structures of ACFH and ACFN may be related to this finding.

The number of acidic and basic groups in all three samples increased; the increase in the number of acidic groups was greater (Table 1). Because the temperature in the plasma channel during pulsed discharge is very high, treatment with oxygen plasma increases the numbers of all chemical groups on the surface, including basic groups [28]. This is in good agreement with the observed decrease in $pH_{PZC}$.

### 3.4. ACF regeneration

The adsorptive capacities of ACF0, ACFH, and ACFN after the sixth cycle were investigated by measuring the amount of MO adsorbed. The initial adsorptive capacities of ACF0, ACFH, and ACFN were 150, 133.6, and 155.6 mg $g^{-1}$, respectively; after the sixth cycle the values were 131.6, 119.6, and 137.9 mg $g^{-1}$. Thus, ACF0, ACFH, and ACFN could be regenerated *in situ* during the combined treatment. ACFH had the largest regeneration rate (89.5%). This can be explained by the increase in its micropores and mesopores, which would increase its adsorption performance.

## 4. Conclusions

Surface modifications of ACF0 led to very different porous structures and chemical properties. Nitric acid oxidation (ACFH) reduced the specific surface area and the micropore and mesopore volumes, and increased the number of acidic groups. Ammonia treatment (ACFN) increased the specific surface area, the micropore and mesopore volumes, and the number of basic groups, and decreased the number of acidic groups.

A synergistic effect appeared in the combined treatment using pulsed discharge and ACF0, ACFH, or ACFN. The disappearance of MO molecules may be caused not only by adsorption on ACF0, ACFH, and ACFN, but also by catalysis. ACF contributed in two ways in pulsed discharge: by acting as an adsorbent that removed a fraction of the unreacted MO molecules and of the by-products produced by degradation of MO; and by acting as a catalyst that promoted decomposition of ozone on the catalyst surface, producing HO• radicals.

Because of surface oxidation in the pulsed discharge process, the surface area and pore volumes of ACFN were altered only slightly after use, but for ACF0 and ACFH these properties were altered significantly. The numbers of acidic groups and basic groups on the ACF0, ACFH, and ACFN surfaces increased. ACF0, ACFH, and ACFN could be regenerated *in situ* in the combined treatment.

## Acknowledgment

This research work is funded by the Education Department of Sichuan Province (08ZA057, 08ZA073).

## References

[1] R. Zhang, C. Zhang, X. Cheng, L. Wang, Y. Wu, Z. Guan, Kinetics of decolorization of azo dye by bipolar pulsed barrier discharge in a three-phase discharge plasma reactor, J. Hazard. Mater. 142 (2007) 105–110.
[2] B. Yang, M. Zhou, L. Lei, Synergistic effects of liquid and gas phase discharges using pulsed high voltage for dyes degradation in the presence of oxygen, Chemosphere 60 (2005) 405–411.
[3] N. Koprivanac, H. Kušić, D. Vujević, I. Peternel, B.R. Locke, Influence of iron on degradation of organic dyes in corona, J. Hazard. Mater. B117 (2005) 113–119.
[4] B.R. Locke, M. Sato, P. Sunka, M.R. Hoffmann, J.-S. Chang, Electrohydraulic discharge and nonthermal plasma for water treatment, Ind. Eng. Chem. Res. 45 (2006) 882–905.
[5] H. Valdés, C.A. Zaror, Ozonation of benzothiazole saturated-activated carbons: influence of carbon chemical surface properties, J. Hazard. Mater. 137 (2006) 1042–1048.
[6] P.C.C. Faria, J.J.M. Órfão, M.F.R. Pereira, Ozonation of aniline promoted by activated carbon, Chemosphere 67 (2007) 809–815.
[7] M. Sánchez-Polo, U. von Gunten, J. Rivera-Utrilla, Efficiency of activated carbon to transform ozone into OH radicals: influence of operational parameters, Water Res. 39 (2005) 3189–3198.
[8] P.M. Alvárez, J.F. García-Araya, F.J. Beltrán, I. Giráldez, J. Jaramillo, V. Gómez-Serrano, The influence of various factors on aqueous ozone decomposition by granular activated carbons and the development of a mechanistic approach, Carbon 44 (2006) 3102–3112.
[9] D.R. Grymonpré, W.C. Finney, B.R. Locke, Aqueous-phase pulsed streamer corona reactor using suspended activated carbon particles for phenol oxidation: model-data comparison, Chem. Eng. Sci. 54 (1999) 3095–3105.
[10] D.R. Grymonpré, A.K. Sharma, W.C. Finney, B.R. Locke, The role of Fenton' s reaction in aqueous phase pulsed streamer corona reactors, Chem. Eng. J. 82 (2001) 189–207.
[11] Y. Zhang, J. Zheng, X. Qu, H. Chen, Effect of granular activated carbon on degradation of methyl orange when applied in combination with high-voltage pulse discharge, J. Colloid Interface Sci. 316 (2007) 523–530.
[12] F.J. López-Garzón, M. Domingo-García, M. Pérez-Mendoza, P.M. Alvarez, V. Gómez-Serrano, Textural and chemical surface modifications produced by some oxidation treatments of a glassy carbon, Langmuir 19 (2003) 2838–2844.
[13] P.M. Álvarez, J.F. García-Araya, F.J. Beltrán, F.J. Masa, F. Medina, Ozonation of activated carbons: effect on the adsorption of selected phenolic compounds from aqueous solutions, J. Colloid Interface Sci. 283 (2005) 503–512.

[14] L.S. Clesceri, A.E. Greenberg, A.D. Eaton, Standard Methods for the Examination of Water and Wastewater, American Public Health Association, New York, 1998.
[15] Y. Zhang, J. Zheng, X. Qu, H. Chen, Design of a novel non-equilibrium plasma-based water treatment reactor, Chemosphere 70 (2008) 1518–1524.
[16] S. Biniak, M. Pakuła, G.S. Szymański, A. Świtkowski, Effect of activated carbon surface oxygen- and/or nitrogen-containing groups on adsorption of copper(II) ions from aqueous solution, Langmuir 15 (1999) 6117–6122.
[17] S. Biniak, G. Szymański, J. Siedlewski, A. Świtkowski, The characterization of activated carbons with oxygen and nitrogen surface groups, Carbon 35 (1997) 1799–1810.
[18] D.B. Mawhinney, J.T. Yates, FTIR study of the oxidation of amorphous carbon by ozone at 300 K-Direct COOH formation, Carbon 39 (2001) 1167–1173.
[19] S. Shin, J. Jang, S.-H. Yoon, I. Mochida, A study on the effect of heat treatment on functional groups of pitch based activated carbon fiber using FTIR, Carbon 35 (1997) 1739–1743.
[20] C. Moreno-Castilla, F. Carrasco-Marín, F.J. Maldonado-Hódar, J. Rivera-Utrilla, Effects of non-oxidant and oxidant acid treatments on the surface properties of an activated carbon with very low ash content, Carbon 36 (1998) 145–151.
[21] M. Domingo-García, F.J. López-Garzón, M. Pérez-Mendoza, Effect of some oxidation treatments on the textural characteristics and surface chemical nature of an activated carbon, J. Colloid Interface Sci. 222 (2000) 233–240.
[22] M. Acedo-Ramos, V. gomez-Serrano, C. Valenzuela-Calahorro, A.J. Lopez-Peinado, Oxidation of activated carbon in liquid phase study by FT-IR, Spectrosc. Lett. 26 (1993) 1117–1137.
[23] E. Fuente, J.A. Menéndez, M.A. Díez, D. Suárez, M.A. Montes-Morán, Infrared spectroscopy of carbon materials: a quantum chemical study of model compounds, J. Phys. Chem. B 107 (2003) 6350–6359.
[24] V. Gómez-Serrano, F. Piriz-Almeida, C.J. Durán-Valle, J. Pastor-Villegas, Formation of oxygen structures by air activation. A study by FT-IR spectroscopy, Carbon 37 (1999) 1517–1528.
[25] J.-W. Shim, S.-J. Park, S.-K. Ryu, Effect of modification with $HNO_3$ and NaOH on metal adsorption by pitch-based activated carbon fibers, Carbon 39 (2001) 1635–1642.
[26] C.L. Mangun, K.R. Benak, J. Economy, K.L. Foster, Surface chemistry, pore sizes and adsorption properties of activated carbon fibers and precursors treated with ammonia, Carbon 39 (2001) 1809–1820.
[27] L.R. Grabowski, E.M.v. Veldhuizen, A.J.M. Pemen, W.R. Rutgers, Breakdown of methylene blue and methyl orange by pulsed corona discharge, Plasma Sources Sci. Technol. 16 (2007) 226–232.
[28] S. Kodama, H. Sekiguchi, Estimation of point of zero charge for activated carbon treated with atmospheric pressure non-thermal oxygen plasmas, Thin Solid Films 506–507 (2006) 327–330.